Analysis of the Inherent Reconstruction Error in Filtered Back Projection

Matthias Beckmann

Department of Mathematics, University of Hamburg

Bundesstraße 55, 20146 Hamburg, Germany

matthias.beckmann@uni-hamburg.de

Armin Iske

Department of Mathematics, University of Hamburg

Bundesstraße 55, 20146 Hamburg, Germany

armin.iske@uni-hamburg.de

Abstract

Computerized tomography allows us to recover bivariate functions from Radon samples. Well-established reconstruction methods are based on the *filtered back projection* (FBP) formula, which yields the analytical inversion of the Radon transform. The FBP formula is, however, highly sensitive with respect to noise and, thus, numerically unstable. To overcome this problem, suitable low-pass filters with compactly supported window functions and of finite bandwidth are employed. The objective of this paper is to analyse the inherent FBP reconstruction error that is incurred when using a low-pass filter of finite bandwidth. To this end, we prove L^2-error estimates for target functions from Sobolev spaces of fractional order. The obtained error bounds are affine-linear with respect to the distance between the filter's window function and the constant function 1 in the L^∞-norm. Our theoretical results are supported by numerical simulations, where in particular the predicted affine-linear behaviour of the error is observed.

1 Introduction

The term *filtered back projection* (FBP) refers to a well-known and commonly used reconstruction technique in computerized tomography (CT), which deals with the generation of medical images from X-ray scans. The development of CT had revolutionary impact in diagnostic medicine, since it provided a non-invasive and safe imaging modality that enabled physicians to view the interior of the human body at high resolution.

The measured X-ray data can be interpreted as a finite set of line integrals of the (unknown) *attenuation function* of the scanned object, which describes the amount of energy being absorbed by the medium. Thus, the CT reconstruction problem of recovering the interior structure of the scanned object from given X-ray scans requires the reconstruction of the object's attenuation function. We can formulate the basic CT reconstruction problem as follows.

Problem 1 (Basic reconstruction problem)**.** *Let $\Omega \subset \mathbb{R}^2$ be a bounded domain. Reconstruct a bivariate function $f \equiv f(x,y)$ with compact support $\mathrm{supp}(f) \subset \Omega$ from its line integrals*

$$\int_\ell f(x,y)\,\mathrm{d}x\,\mathrm{d}y$$

for all straight lines $\ell \subset \mathbb{R}^2$ passing through Ω. ∎

To parametrize straight lines in the plane, let $\ell_{t,\theta}$ denote the unique straight line which passes through the point $(t\cos(\theta), t\sin(\theta)) \in \mathbb{R}^2$, for $(t,\theta) \in \mathbb{R} \times [0,\pi)$, and is perpendicular to the unit vector $\mathbf{n}_\theta = (\cos(\theta), \sin(\theta))$. In this case, $\ell_{t,\theta}$ has distance $|t|$ to the origin. Moreover, every straight line $\ell \subset \mathbb{R}^2$ can uniquely be represented by one parameter pair $(t,\theta) \in \mathbb{R} \times [0,\pi)$, so that $\ell \equiv \ell_{t,\theta}$. This allows us to reformulate the basic reconstruction problem accordingly.

To this end, we regard for $f \in \mathrm{L}^1(\mathbb{R}^2)$ its *Radon transform* $\mathcal{R}f$, given by

$$\mathcal{R}f(t,\theta) = \int_{\ell_{t,\theta}} f(x,y)\,\mathrm{d}x\,\mathrm{d}y \quad \text{for } (t,\theta) \in \mathbb{R} \times [0,\pi).$$

Note that the Radon transform $\mathcal{R}$ maps a bivariate function $f \equiv f(x,y)$ in Cartesian coordinates onto a bivariate function $\mathcal{R}f \equiv \mathcal{R}f(t,\theta)$ in polar coordinates, where $\mathcal{R}f(t,\theta)$ represents the line integral of f over $\ell_{t,\theta}$. Therefore, the basic reconstruction problem, Problem 1, seeks for the inversion of the Radon transform $\mathcal{R}f$ from input Radon data $\{\mathcal{R}f(t,\theta) \mid t \in \mathbb{R}, \theta \in [0,\pi)\}$. For a comprehensive mathematical treatment of the Radon transform and its inversion, we refer to the textbooks [3, 8].

The outline of this paper is as follows. In Section 2, we briefly review the inversion of the Radon transform by the FBP formula. Moreover, we explain how the FBP can be stabilized by using a suitable *low-pass filter* with a compactly supported window function and of finite bandwidth. This stabilization modifies the FBP formula, leading to an *approximate* FBP reconstruction formula, whose evaluation requires a rigorous analysis of the approximation error being incurred by the application of a low-pass filter. Error bounds depending on the utilized filter's window function, along with its bandwidth, and on the regularity of the target function are of particular interest. To this end, in Section 3 we prove suitable error bounds with respect to the L^2-norm and for target functions from Sobolev spaces of fractional order. The resulting L^2-error estimates, as summarized by Theorem 1 and first presented in [1], are, to the best of our knowledge, new. Supporting numerical simulations are finally provided in Section 4.

2   Filtered Back Projection

The analytical inversion of the Radon transform $\mathcal{R}$ is well understood. It involves the (continuous) *Fourier transform* on $\mathbb{R}$, here taken as

$$\mathcal{F}g(S,\theta) = \int_{\mathbb{R}} g(t,\theta)\,\mathrm{e}^{-\mathrm{i}tS}\,\mathrm{d}t \quad \text{for } (S,\theta) \in \mathbb{R} \times [0,\pi)$$

for $g \equiv g(t,\theta)$ satisfying $g(\cdot,\theta) \in \mathrm{L}^1(\mathbb{R})$ for all $\theta \in [0,\pi)$, in combination with the *back projection*

$$\mathcal{B}h(x,y) = \frac{1}{\pi} \int_0^{\pi} h(x\cos(\theta) + y\sin(\theta), \theta)\,\mathrm{d}\theta \quad \text{for } (x,y) \in \mathbb{R}^2$$

for $h \in \mathrm{L}^1(\mathbb{R} \times [0,\pi))$. Note that the back projection operator $\mathcal{B}$ is the adjoint operator of $\mathcal{R}$, which maps a bivariate function $h \equiv h(t,\theta)$ in polar coordinates onto a bivariate function $\mathcal{B}h \equiv \mathcal{B}h(x,y)$ in Cartesian coordinates.

Later in this paper, we also work with the *Fourier transform* on $\mathbb{R}^2$, defined as

$$\mathcal{F}f(X,Y) = \int_{\mathbb{R}^2} f(x,y)\,\mathrm{e}^{-\mathrm{i}(xX+yY)}\,\mathrm{d}x\,\mathrm{d}y \quad \text{for } (X,Y) \in \mathbb{R}^2,$$

for $f \equiv f(x,y)$ in Cartesian coordinates, where we assume $f \in \mathrm{L}^1(\mathbb{R}^2)$.

Now the inversion of the Radon transform is given by the classical *filtered back projection formula* (see e.g. [2, Theorem 6.2.])

$$f(x,y) = \frac{1}{2}\,\mathcal{B}\left(\mathcal{F}^{-1}[|S|\mathcal{F}(\mathcal{R}f)(S,\theta)]\right)(x,y) \quad \text{for all } (x,y) \in \mathbb{R}^2, \qquad (1)$$

which holds for any function $f \in \mathrm{L}^1(\mathbb{R}^2) \cap \mathcal{C}(\mathbb{R}^2)$.

By the application of the filter $|S|$ to the Fourier transform $\mathcal{F}(\mathcal{R}f)$ in (1), especially the high frequency components of $\mathcal{R}f$ are amplified by the magnitude of $|S|$. Therefore, the filtered back projection formula is in particular highly sensitive with respect to noise and, thus, numerically *unstable*. Needless to say that this is critical in many relevant applications, where a reconstruction by FBP would lead to an undesired corruption of the image.

To reduce the sensitivity of the FBP formula with respect to noise, we follow a standard approach and replace the filter $|S|$ in (1) by a suitable *low-pass filter* $A_L : \mathbb{R} \longrightarrow \mathbb{R}$ of the form

$$A_L(S) = |S|W(S/L)$$

with finite *bandwidth $L > 0$* and an even *window function $W : \mathbb{R} \longrightarrow \mathbb{R}$* with compact support $\mathrm{supp}(W) \subseteq [-1,1]$. Further, we assume $W \in \mathrm{L}^1(\mathbb{R})$. Therefore, the scaled window function $W_L(S) = W(S/L)$ is even and compactly supported with $\mathrm{supp}(W_L) \subseteq [-L,L]$. In particular, $W_L \in \mathrm{L}^1(\mathbb{R})$, and so any low-pass filter of the form $A_L(S) = |S|W_L(S)$ is in $\mathrm{L}^1(\mathbb{R})$, unlike $|S|$.

When replacing the filter $|S|$ in (1) with the low-pass filter A_L, the reconstruction of f is no longer exact and we only get an approximate FBP reconstruction, here denoted by f_L. In this case, the resulting *approximate FBP formula* can be simplified as

$$f_L(x,y) = \frac{1}{2} \mathcal{B} \left(\mathcal{F}^{-1}[A_L(S)\mathcal{F}(\mathcal{R}f)(S,\theta)] \right)(x,y) = \frac{1}{2} \mathcal{B} \left(\mathcal{F}^{-1}A_L * \mathcal{R}f \right)(x,y),$$

where $*$ denotes the convolution product on $\mathbb{R}$, here taken as

$$(g*h)(S,\theta) = \int_{\mathbb{R}} g(t,\theta)\, h(S-t,\theta)\, \mathrm{d}t \quad \text{for } (S,\theta) \in \mathbb{R} \times [0,\pi)$$

for $g \equiv g(t,\theta)$ and $h \equiv h(t,\theta)$ in polar coordinates, where we require that both $g(\cdot,\theta)$ and $h(\cdot,\theta)$ are integrable on $\mathbb{R}$ for all $\theta \in [0,\pi)$.

We can further simply this representation of f_L by involving the band-limited function

$$q_L(t,\theta) = \mathcal{F}^{-1}A_L(t) \quad \text{for } (t,\theta) \in \mathbb{R} \times [0,\pi),$$

in which case we get

$$f_L = \frac{1}{2} \mathcal{B}(q_L * \mathcal{R}f). \tag{2}$$

For the sake of brevity, we call any application of the approximate FBP formula (2) an *FBP method*. Thus, each FBP method yields one approximation f_L to f, $f_L \approx f$, whose quality depends on the choice of the low-pass filter A_L.

In the following, we analyse the inherent error of the FBP method being incurred by the chosen low-pass filter A_L of finite bandwidth L, i.e., we wish to analyse the error

$$e_L = f - f_L. \tag{3}$$

We remark that pointwise and L^∞-error estimates on e_L were proven by Munshi et al. in [5]. Their results are further supported by numerical experiments in [6]. Error bounds on the L^p-norm of e_L, in terms of an L^p-modulus of continuity of the target function f, were proven by Madych in [4].

We remark that the approach taken in this paper is essentially different from previous approaches, in particular different from that in [4]. To further explain this, we prove L^2-error estimates on e_L for the relevant case of target functions f from Sobolev spaces of fractional order. Here, the *Sobolev space* $\mathrm{H}^\alpha(\mathbb{R}^2)$ of order $\alpha \in \mathbb{R}$ is defined as

$$\mathrm{H}^\alpha(\mathbb{R}^2) = \left\{ f \in \mathcal{S}'(\mathbb{R}^2) \mid \|f\|_\alpha < \infty \right\},$$

whose norm $\| \cdot \|_\alpha$ is given by

$$\|f\|_\alpha^2 = \frac{1}{2\pi} \int_{\mathbb{R}} \int_{\mathbb{R}} \left(1 + x^2 + y^2\right)^\alpha |\mathcal{F}f(x,y)|^2\, \mathrm{d}x\, \mathrm{d}y,$$

and where $\mathcal{S}'(\mathbb{R}^2)$ denotes the usual space of tempered distributions on $\mathbb{R}^2$, with respect to the Schwartz space $\mathcal{S}$. It can be shown that for any non-negative integer $\alpha \in \mathbb{N}_0$ the Sobolev space $\mathrm{H}^\alpha(\mathbb{R}^2)$ consists of functions, all of whose (distributional) derivatives up to order α are square-integrable. Thus, for $\alpha \in \mathbb{N}_0$ the above definition is consistent with the usual definition of Sobolev spaces via weak differentiability.

In the relevant application of (medical) image processing, Sobolev spaces of compactly supported functions on a bounded domain $\Omega \subset \mathbb{R}^2$, and of fractional order $\alpha \in \mathbb{R}$,

$$\mathrm{H}_0^\alpha(\Omega) = \left\{ f \in \mathrm{H}^\alpha(\mathbb{R}^2) \mid \mathrm{supp}(f) \subseteq \overline{\Omega} \right\},$$

play an important role (cf. [7]). In fact, a density function f of an image in $\Omega \subset \mathbb{R}^2$ has usually jumps along smooth curves, but is otherwise smooth off these curve singularities. Such functions belong to a Sobolev space $\mathrm{H}_0^\alpha(\mathbb{R}^2)$ for $\alpha < 1/2$. Thus, we can describe the density of an image as a function in a Sobolev space $\mathrm{H}_0^\alpha(\Omega)$ whose order α is close to $1/2$.

3 Analysis of the FBP Reconstruction Error

In this section we prove L^2-estimates for the intrinsic FBP reconstruction error e_L in (3), where our upper bound on the L^2-norm of e_L will be split into one error term depending on the filter's window function W and another one depending on its bandwidth $L > 0$.

Let us first discuss the special case of the *Ram-Lak filter*, given as

$$A_L(S) = \left\{ \begin{array}{ll} |S| & \text{for } S \in [-L, L], \\ 0 & \text{otherwise.} \end{array} \right.$$

Note that the Ram-Lak filter's window function W is given by the characteristic function $\chi_{[-1,1]}$ of the interval $[-1, 1]$, so that the scaled window function W_L is the characteristic function $\chi_{[-L,L]}$ of the interval $[-L, L]$. From this observation, we see that the reconstruction error e_L vanishes identically, $e_L \equiv 0$, for target functions f with band-limited Radon transform $\mathcal{R}f$, provided that the band-width L is at least as large as the largest frequency contained in $\mathcal{R}f$. Indeed, in this case the approximate Ram-Lak FBP formula (2) coincides with the exact FBP formula (1), so that $f \equiv f_L$.

Yet it remains to discuss how reasonable it is to assume that the target function f has a band-limited Radon transform $\mathcal{R}f$. To further elaborate this, let us recall the standard *central slice theorem* (see e.g. [2, Theorem 6.1.]), which states that for any $f \in \mathrm{L}^1(\mathbb{R}^2) \cap \mathcal{C}(\mathbb{R}^2)$ the identity

$$\mathcal{F}(\mathcal{R}f)(S, \theta) = \mathcal{F}f(S\cos(\theta), S\sin(\theta)) \tag{4}$$

holds for all $(S, \theta) \in \mathbb{R} \times [0, \pi)$. Hence, the (univariate) Fourier transform of $\mathcal{R}f$ is entirely determined by the (bivariate) Fourier transform of f, and vice versa.

Now, $\mathcal{R}f$ is band-limited if and only if $\mathcal{R}f$ has a compactly supported Fourier transform $\mathcal{F}(\mathcal{R}f)$. However, for applications of medical image reconstruction, it is usually assumed that $f \not\equiv 0$ is compactly supported. But in this case, its Fourier transform $\mathcal{F}f$ is analytic, due to the well-known *Paley-Wiener theorem* (see e.g. [9, Theorem 7.22]), and so is $\mathcal{F}(\mathcal{R}f)$ an analytic function, by the central slice theorem (4). Hence, $\mathcal{F}(\mathcal{R}f)$ cannot be compactly supported, i.e., $\mathcal{R}f$ cannot be band-limited.

To conclude our discussion on the special case of the Ram-Lak filter, we see that, for compactly supported $f \not\equiv 0$, the error e_L of the Ram-Lak FBP method cannot be zero for finite bandwidth $L > 0$. But if we let L go to infinity, the Ram-Lak FBP method will coincide, in the limit, with the exact, but numerically unstable filtered back projection formula (1), i.e., $e_\infty \equiv 0$. In other words, any admissible target function f can be approximated arbitrarily well by f_L for sufficiently large L.

Before we turn to error estimates on e_L, it is convenient to rewrite the approximate reconstruction formula (2) in terms of the target function f. To be more precise, we seek for a function $K_L : \mathbb{R}^2 \longrightarrow \mathbb{R}$ satisfying

$$f_L = f * K_L,$$

where $*$ now denotes the usual convolution product on $\mathbb{R}^2$, defined as

$$(g * h)(X, Y) = \int_{\mathbb{R}^2} g(x, y)\, h(X - x, Y - y)\, \mathrm{d}x\, \mathrm{d}y \quad \text{for } (X, Y) \in \mathbb{R}^2$$

for $g \equiv g(x, y)$ and $h \equiv h(x, y)$ in Cartesian coordinates satisfying $g, h \in \mathrm{L}^1(\mathbb{R}^2)$. This relation plays a central role in our error analysis. The construction of such a function K_L is based on the following standard relation between the convolution product $*$, the back projection operator $\mathcal{B}$, and the Radon transform $\mathcal{R}$, as detailed in the textbook [8] of Natterer (see [8, Theorem II.1.3]).

Lemma 1. *Let $f \equiv f(x, y) \in \mathrm{L}^1(\mathbb{R}^2)$ be a bivariate function in Cartesian coordinates and let $g \equiv g(t, \theta)$ be a bivariate function in polar coordinates satisfying $g(\cdot, \theta) \in \mathrm{L}^1(\mathbb{R})$ for all $\theta \in [0, \pi)$. Then, the identity*

$$(\mathcal{B}g * f)(X, Y) = \mathcal{B}(g * \mathcal{R}f)(X, Y) \tag{5}$$

holds for all $(X, Y) \in \mathbb{R}^2$.

Although formula (5) belongs to the standard repertoire of CT techniques, we give a proof for the reader's convenience.

Proof. For $(X, Y) \in \mathbb{R}^2$, we have

$$(\mathcal{B}g * f)(X, Y) = \int_{\mathbb{R}} \int_{\mathbb{R}} \mathcal{B}g(X - x, Y - y)\, f(x, y)\, \mathrm{d}x\, \mathrm{d}y,$$

where, with letting $\bar{x} = X - x$ and $\bar{y} = Y - y$, we obtain

$$\mathcal{B}g(\bar{x}, \bar{y}) = \frac{1}{\pi} \int_0^\pi g(\bar{x}\cos(\theta) + \bar{y}\sin(\theta), \theta) \, \mathrm{d}\theta.$$

By applying the substitutions

$$x = t\cos(\theta) - s\sin(\theta)$$
$$y = t\sin(\theta) + s\cos(\theta),$$

we get $\mathrm{d}x\,\mathrm{d}y = \mathrm{d}s\,\mathrm{d}t$ and, therefore, with

$$\mathcal{R}f(t, \theta) = \int_\mathbb{R} f(t\cos(\theta) - s\sin(\theta), t\sin(\theta) + s\cos(\theta)) \, \mathrm{d}s$$

and $s_\theta = X\cos(\theta) + Y\sin(\theta)$, we can conclude

$$\begin{aligned}
(\mathcal{B}g * f)(X, Y) &= \frac{1}{\pi} \int_0^\pi \int_\mathbb{R} g(s_\theta - t, \theta)\,\mathcal{R}f(t, \theta)\,\mathrm{d}t\,\mathrm{d}\theta \\
&= \frac{1}{\pi} \int_0^\pi (g * \mathcal{R}f)(s_\theta, \theta)\,\mathrm{d}\theta \\
&= \mathcal{B}(g * \mathcal{R}f)(X, Y),
\end{aligned}$$

as stated. $\qquad\square$

Now for $q_L \in \mathrm{L}^1(\mathbb{R} \times [0, \pi))$, we define the *convolution kernel* $K_L : \mathbb{R}^2 \longrightarrow \mathbb{R}$ by

$$K_L(x, y) = \frac{1}{2}\mathcal{B}q_L(x, y) \quad \text{for } (x, y) \in \mathbb{R}^2, \tag{6}$$

so that, from Lemma 1, we obtain the desired representation for the approximate reconstruction f_L by

$$f_L(x, y) = \frac{1}{2}\mathcal{B}(q_L * \mathcal{R}f)(x, y) = (f * K_L)(x, y) \tag{7}$$

for all $(x, y) \in \mathbb{R}^2$.

Let us now turn to the analysis of the reconstruction error in the L^2-norm. To this end, we assume $f \in \mathrm{L}^1(\mathbb{R}^2) \cap \mathrm{L}^2(\mathbb{R}^2)$, in which case we get

$$\|f - f_L\|_{\mathrm{L}^2(\mathbb{R}^2)}^2 = \|f - f * K_L\|_{\mathrm{L}^2(\mathbb{R}^2)}^2 = \frac{1}{2\pi}\|\mathcal{F}f - \mathcal{F}f \cdot \mathcal{F}K_L\|_{\mathrm{L}^2(\mathbb{R}^2;\mathbb{C})}^2,$$

from the representation (7) for f_L. Further, we applied the Rayleigh-Plancherel theorem, which states that the Fourier transform $\mathcal{F}$ is an isometry on $\mathrm{L}^2(\mathbb{R}^2)$, in our case up to the multiplicative constant $(2\pi)^{-1/2}$.

By letting $W_L(x, y) = W_L(r(x, y))$ for $r(x, y) = \sqrt{x^2 + y^2}$ and $(x, y) \in \mathbb{R}^2$, we obtain a radially symmetric bivariate function $W_L : \mathbb{R}^2 \longrightarrow \mathbb{R}$. It can be

shown that the Fourier transform of the convolution kernel K_L in (6) is given
by the bivariate radial window function W_L, i.e., for $K_L \in \mathrm{L}^1(\mathbb{R}^2)$ we have

$$\mathcal{F}K_L(x,y) = W_L(x,y) \quad \text{for all } (x,y) \in \mathbb{R}^2,$$

in consequence of [8, Theorem II.1.4]. But this implies

$$\|e_L\|_{\mathrm{L}^2(\mathbb{R}^2)}^2 = \frac{1}{2\pi}\|\mathcal{F}f - W_L \cdot \mathcal{F}f\|_{\mathrm{L}^2(\mathbb{R}^2;\mathbb{C})}^2 = \frac{1}{2\pi}\int_\mathbb{R}\int_\mathbb{R}|(\mathcal{F}f - W_L \cdot \mathcal{F}f)(x,y)|^2 \mathrm{d}x\,\mathrm{d}y.$$

To continue with our analysis, we split the above representation of the L^2-norm
$\|e_L\|_{\mathrm{L}^2(\mathbb{R}^2)}$ of the error e_L into a sum of two integrals,

$$\|e_L\|_{\mathrm{L}^2(\mathbb{R}^2)}^2 = I_1 + I_2,$$

where

$$I_1 = \frac{1}{2\pi}\int_{\|\binom{x}{y}\|_2 \leq L}|(\mathcal{F}f - W_L \cdot \mathcal{F}f)(x,y)|^2\,\mathrm{d}x\,\mathrm{d}y,$$

$$I_2 = \frac{1}{2\pi}\int_{\|\binom{x}{y}\|_2 > L}|\mathcal{F}f(x,y)|^2\,\mathrm{d}x\,\mathrm{d}y.$$

We now analyse these two error terms separately. Note that the first error term
I_1 occurs if the chosen window function W is not constant 1, $W \not\equiv 1$, on $[-1,1]$.
To estimate the integral I_1, we consider a fixed low-pass filter $A_L(S) = |S|W_L(S)$
with a bounded window function $W \in \mathrm{L}^\infty(\mathbb{R})$. Then, for $f \in \mathrm{L}^1(\mathbb{R}^2) \cap \mathrm{L}^2(\mathbb{R}^2)$,
the integral I_1 can be bounded above by

$$I_1 = \frac{1}{2\pi}\int_{r(x,y)\leq L}\left(1 - W_L(r(x,y))\right)^2|\mathcal{F}f(x,y)|^2\,\mathrm{d}x\,\mathrm{d}y$$

$$\leq \|1 - W_L\|_{\infty,[-L,L]}^2\frac{1}{2\pi}\int_\mathbb{R}\int_\mathbb{R}|\mathcal{F}f(x,y)|^2\,\mathrm{d}x\,\mathrm{d}y$$

$$= \|1 - W\|_{\infty,[-1,1]}^2\|f\|_{\mathrm{L}^2(\mathbb{R}^2)}^2,$$

since

$$\|1 - W_L\|_{\infty,[-L,L]} = \|1 - W\|_{\infty,[-1,1]}$$

and

$$\frac{1}{2\pi}\|f\|_{\mathrm{L}^2(\mathbb{R}^2;\mathbb{C})}^2 = \|f\|_{\mathrm{L}^2(\mathbb{R}^2)}^2,$$

where we applied the Rayleigh-Plancherel theorem once more.

The second error term I_2 occurs if the target function f is not band-limited.
We recall that this is usually the case for applications of medical image recon-
struction. To estimate the integral I_2, we now assume that the target function f

belongs to a Sobolev space of positive fractional order. In fact, for $f \in \mathrm{H}^\alpha(\mathbb{R}^2)$, with $\alpha > 0$, the integral I_2 can be bounded above by

$$
\begin{aligned}
I_2 &= \frac{1}{2\pi} \int_{r(x,y)>L} \left(1 + x^2 + y^2\right)^\alpha \left(1 + x^2 + y^2\right)^{-\alpha} |\mathcal{F}f(x,y)|^2 \, \mathrm{d}x \, \mathrm{d}y \\
&\leq \frac{1}{2\pi} \int_{r(x,y)>L} \left(1 + x^2 + y^2\right)^\alpha L^{-2\alpha} |\mathcal{F}f(x,y)|^2 \, \mathrm{d}x \, \mathrm{d}y \\
&\leq L^{-2\alpha} \|f\|_\alpha^2 .
\end{aligned}
$$

We can summarize our discussion of this section as follows.

Theorem 1 (L^2-error estimate)**.** *Let $f \in \mathrm{L}^1(\mathbb{R}^2) \cap \mathrm{H}^\alpha(\mathbb{R}^2)$ for some $\alpha > 0$, let $W \in \mathrm{L}^\infty(\mathbb{R})$ be even and compactly supported with $\mathrm{supp}(W) \subseteq [-1,1]$, and let $K_L \in \mathrm{L}^1(\mathbb{R}^2)$. Then, the L^2-norm of the FBP reconstruction error $e_L = f - f_L$ in (3) is bounded above by*

$$
\|e_L\|_{\mathrm{L}^2(\mathbb{R}^2)} \leq \|1 - W\|_{\infty,[-1,1]} \|f\|_{\mathrm{L}^2(\mathbb{R}^2)} + L^{-\alpha} \|f\|_\alpha \tag{8}
$$

for all $L > 0$. $\square$

We can conclude that the choice of both the window function W and the bandwidth L are of fundamental importance for the L^2-error of the FBP method. In fact, for any target function f and bandwidth L, the obtained error estimate is affine-linear with respect to the L$^\infty$-distance between the window function W and the constant function 1 on the interval $[-1,1]$. This relation will also be observed numerically in the following section.

Moreover, the error term $\|1 - W\|_{\infty,[-1,1]}$ can be used to evaluate the quality of the window W. Note that the window function $W \equiv \chi_{[-1,1]}$ of the Ram-Lak filter is the unique minimizer of that quality indicator, and so the Ram-Lak filter is in this sense the *optimal* low-pass filter.

Finally, note that the smoothness α of f determines the decay rate of the second error term by

$$
L^{-\alpha} \|f\|_\alpha = \mathcal{O}(L^{-\alpha}) \quad \text{for } L \longrightarrow \infty .
$$

However, our L^2-error bound in (8) can only tend to zero if we choose the Ram-Lak filter with window $W = \chi_{[-1,1]}$ and let L go to ∞. This observation complies with the derived conditions under which we achieve an exact reconstruction of the target function f by the FBP formula (1), as this is explained at the outset of this section.

4   Numerical Experiments

In this section, we finally present selected numerical examples to evaluate the FBP reconstruction error numerically and to validate our L^2-error estimate (8).

First note that the approximate FBP reconstruction formula assumes the Radon data $\mathcal{R}f(t, \theta)$ to be available for all $(t, \theta) \in \mathbb{R} \times [0, \pi)$. In practice, however, only finitely many Radon samples are given. For *parallel beam geometry* (cf. [2]) the input Radon data are usually of the form

$$(\mathcal{R}f)_{j,k} = \mathcal{R}f(t_j, \theta_k) \tag{9}$$

for $-M \le j \le M$ and $0 \le k \le N-1$ for $M, N \in \mathbb{N}$. The reconstruction of f from Radon data (9) requires a suitable *discretization* of the FBP method (2), leading to inevitable discretization errors that are not covered by our error analysis.

To implement the approximate FBP reconstruction formula

$$f_L = \frac{1}{2} \mathcal{B} \left(\mathcal{F}^{-1} A_L * \mathcal{R}f \right),$$

we need to discretize the back projection $\mathcal{B}$, the inverse Fourier transform $\mathcal{F}^{-1}$, the convolution product $*$ and the Radon transform $\mathcal{R}$. For the sake of brevity, we refrain from explaining their discretizations. Instead, we rather refer to [2, Chapter 8]. For the purpose of this paper, it is sufficient to say that we rely on parallel beam geometry (9), where the parameter M depends on the bandwidth L of the low-pass filter A_L, according to the Nyquist sampling theorem (cf. [2]).

In our numerical experiments, we used the popular *Shepp-Logan phantom*. For this test case, the Radon transform can be calculated analytically. Therefore, the Shepp-Logan phantom's Radon data are exact, so that the observed errors are due to the discretized approximate reconstruction method. The Shepp-Logan phantom consists of ten ellipses of constant densities, but different sizes, eccentricities and locations, see Figure 1(a). The phantom was introduced by Shepp and Logan [10] to simulate a cross-section of the human head. For our numerical experiments, we modified the densities of the different ellipses from the original Shepp-Logan phantom in order to get a higher contrast in the image for a better visual perception.

Figure 1(c) shows the corresponding sinogram, i.e., the Radon data of the phantom in the (t, θ)-plane. The FBP reconstruction based on this test case is displayed in Figure 1(b), where we used the Shepp-Logan filter with window

$$W(S) = \operatorname{sinc}(\pi S/2) \cdot \chi_{[-1,1]}(S),$$

bandwidth $L = 20$ and $N = 60$ for the number of angles.

To measure the reconstruction error, we used the standard *root mean square error* (RMSE), which is defined for images with $J \times K$ pixels as

$$\text{RMSE} = \sqrt{\frac{1}{J \times K} \sum_{j=1}^{J} \sum_{k=1}^{K} \left(f_{j,k} - (f_L)_{j,k} \right)^2}.$$

In our numerical experiments, we evaluated the Shepp-Logan phantom and its FBP reconstructions on a square grid with 256×256 pixels.

(a) Phantom
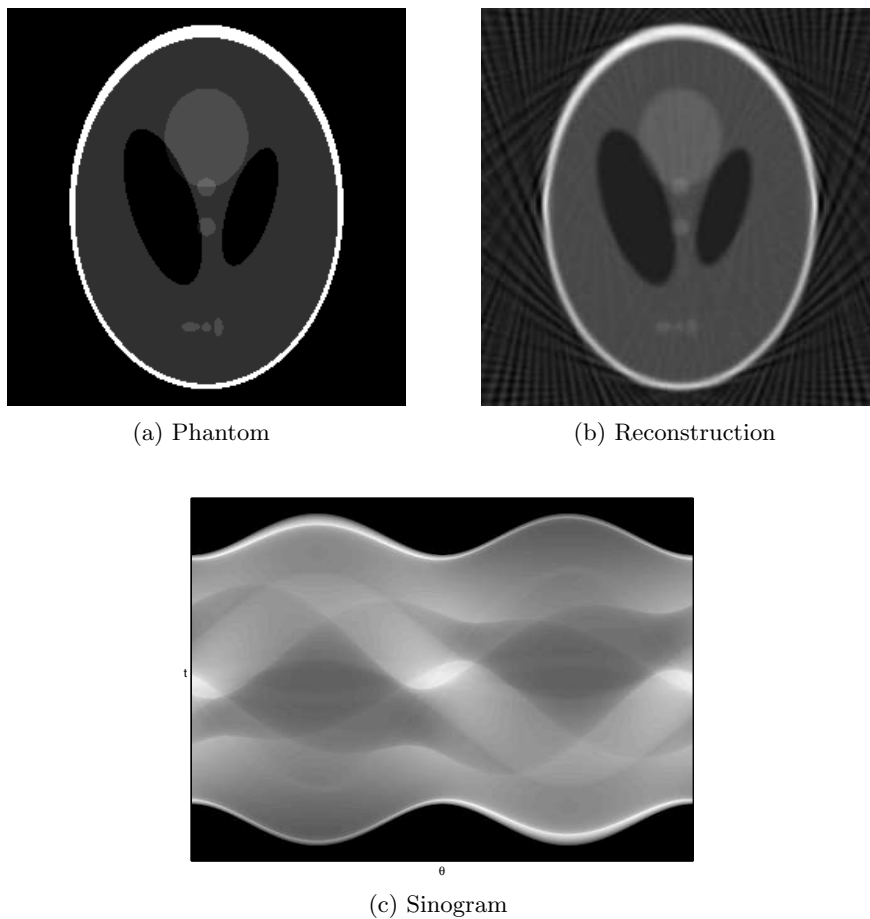
(b) Reconstruction

(c) Sinogram

Figure 1: Reconstruction of the Shepp-Logan phantom.

For the numerical evaluation of the FBP method (2), the intrinsic error of the reconstruction, which is incurred by the application of the low-pass filter A_L with finite bandwidth L, is of primary interest.

Our L^2-error estimate (8) states that, for any target $f \in L^1(\mathbb{R}^2) \cap H^\alpha(\mathbb{R}^2)$ with smoothness $\alpha > 0$, the FBP reconstruction error is bounded above by

$$\|f - f_L\|_{L^2(\mathbb{R}^2)} \leq \|1 - W\|_{\infty,[-1,1]} \|f\|_{L^2(\mathbb{R}^2)} + L^{-\alpha} \|f\|_\alpha.$$

Here, we see that, for fixed function f and bandwidth L, the performance of the chosen low-pass filter A_L is governed by the L^∞-distance between its window function W and the constant function 1 on the interval $[-1, 1]$. Moreover, the error formula predicts an affine-linear behaviour of the error e_L with respect to the quality indicator $\|1 - W\|_{\infty,[-1,1]}$. To investigate the error e_L numerically, we have employed four commonly used low-pass filters $A_L(S) = |S|W(S/L)$:

Name	$W(S)$ for $|S| \leq 1$	$\|1 - W\|_{\infty,[-1,1]}$	Parameter
Ram-Lak	1	0	$-$
Shepp-Logan	$\mathrm{sinc}(\pi S/2)$	$1 - 2/\pi$	$-$
Hamming	$\beta + (1 - \beta) \cos(\pi S)$	$2(1 - \beta)$	$\beta \in \left[\frac{1}{2}, 1\right]$
Gaussian	$\exp\!\left(-(\pi S/\beta)^2\right)$	$1 - \exp(-\pi^2/\beta^2)$	$\beta > 1$

Note that each window function W has compact support $\mathrm{supp}(W) = [-1, 1]$, and so we have $\mathrm{supp}(W_L) = [-L, L]$.

In addition to the popular Ram-Lak and Shepp-Logan filters, we applied the Hamming filter for different choices of parameters $\beta \in \left[\frac{1}{2}, 1\right]$, namely for $\beta \in \{0.5 + 0.05 \cdot j \mid 0 \leq j \leq 10\} \cup \{0.92\}$. This decision was taken in order to work with a sequence of filters of the same form, but with different values for the quality indicator $\|1 - W\|_{\infty,[-1,1]}$.

As suggested in [6], we also included the Gaussian filter for different choices of the parameter $\beta > 1$, here for $\beta \in \{2, 4.7, 7.5, 10, 15\}$. For $\beta = 4.7$, the Gaussian filter and the Shepp-Logan filter have the same value for $\|1 - W\|_{\infty,[-1,1]}$. Hence, the corresponding reconstruction errors should behave similarly due to our error estimate (8). Figure 2 shows, for the test case of the Shepp-Logan phantom, the RMSE as a function of $\|1 - W\|_{\infty,[-1,1]}$ for different choices of the bandwidth L and number of views N.

We can explain the results of our numerical experiments as follows.

First we observe an increasing RMSE when increasing the quality indicator $\|1 - W\|_{\infty,[-1,1]}$ in all of our numerical experiments. This is exactly the behaviour we expected, due to the first error term in our L²-error estimate, given as

$$\|1 - W\|_{\infty,[-1,1]} \, \|f\|_{L^2(\mathbb{R}^2)}.$$

Moreover, the predicted affine-linear behaviour of the RMSE with respect to $\|1 - W\|_{\infty,[-1,1]}$ is clearly visible (see Figure 2). As expected, the RMSE of the Gaussian filter with $\beta = 4.7$ and the Shepp-Logan filter are nearly the same in all our test case scenarios.

Secondly, we see that the RMSE decreases at increasing bandwidth L. This behaviour complies with the second error term in our L²-error estimate,

$$L^{-\alpha} \, \|f\|_{\alpha} \quad \text{for } \alpha > 0.$$

In more details, comparing our numerical results for an equal number of views $N = 30$ but for different bandwidths, $L = 12$ (Figure 2(a)) and $L = 16$ (Figure 2(b)), we see that the RMSE decreases for all filters, as predicted by our error estimate. Further, the affine-linear behaviour of the RMSE with respect to $\|1 - W\|_{\infty,[-1,1]}$ is clearly visible for the parameter choices $L = 12$ and $N = 30$. For $L = 16$ and $N = 30$, however, the affine linearity is slightly disturbed.
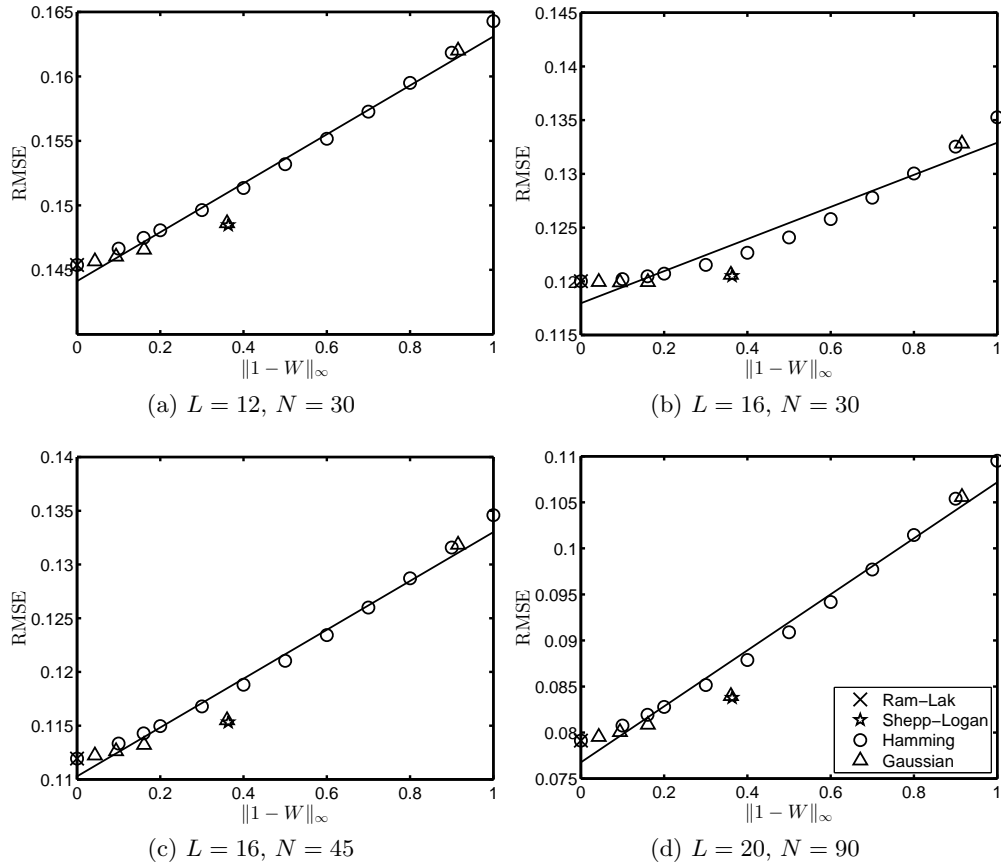
Figure 2: RMSE for the Shepp-Logan phantom.

When increasing the number of views from $N = 30$ to $N = 45$, at fixed bandwidth $L = 16$, we see that the RMSE decreases further (see Figure 2(c)). Moreover, the affine-linear behaviour of the RMSE is more pronounced.

We remark that the value of N does not contribute to the intrinsic FBP reconstruction error, but it rather affects the discretization error. By increasing N, the discretization error is reduced. This is necessary for larger bandwidths L, since in that case the intrinsic error is small, so that a finer discretization can contribute more to the reduction of the RMSE. This can be seen in Figure 2(d), where we chose the bandwidth $L = 20$ and the number of views $N = 90$.

5 Conclusion

In this paper, we considered the inherent FBP reconstruction error $e_L = f - f_L$ being incurred by the use of a low-pass filter A_L with a compactly supported

window function W and of finite bandwidth L. We proved the L^2-error estimate

$$\|e_L\|_{\mathrm{L}^2(\mathbb{R}^2)} \le \|1 - W\|_{\infty,[-1,1]}\, \|f\|_{\mathrm{L}^2(\mathbb{R}^2)} + L^{-\alpha}\, \|f\|_\alpha,$$

which consists of two error terms: The first one only depends on the choice of the filter's window function W, whereas the second one is only dependent on the filter's bandwidth L. Here, the smoothness α of the target function f determines the decay rate of the second error term. Moreover, the obtained error estimate is affine-linear with respect to the magnitude of $\|1 - W\|_{\infty,[-1,1]}$ and this term can be used to evaluate the approximation quality of the window W. Our results are supported by numerical experiments using the Shepp-Logan phantom, where the affine-linear behaviour of the error with respect to $\|1 - W\|_{\infty,[-1,1]}$ is observed.

References

[1] M. Beckmann and A. Iske: Error estimates for filtered back projection. *IEEE 2015 International Conference on Sampling Theory and Applications (SampTA 2015)*, 553–557, 2015.

[2] T.G. Feeman: *The Mathematics of Medical Imaging: A Beginner's Guide.* Second Edition. Springer Undergraduate Texts in Mathematics and Technology (SUMAT), Springer, New York, 2015.

[3] S. Helgason: *The Radon Transform.* Progress in Mathematics, vol. 5, Birkhäuser, Boston, 1999.

[4] W.R. Madych: Summability and approximate reconstruction from Radon transform data. In: *Integral Geometry and Tomography*, E. Grinberg and T. Quinto (eds.), Amer. Math. Soc., Providence, 189–219, 1990.

[5] P. Munshi, R.K.S. Rathore, K.S. Ram, and M.S. Kalra: Error estimates for tomographic inversion. *Inverse Problems* **7**(3), 399–408, 1991.

[6] P. Munshi, R.K.S. Rathore, K.S. Ram, and M.S. Kalra: Error analysis of tomographic filters II: results, *NDT & E Int.* **26**(5), 235–240, 1993.

[7] F. Natterer: A Sobolev space analysis of picture reconstruction. *SIAM J. Appl. Math.* **39**(3), 402–411, 1980.

[8] F. Natterer: *The Mathematics of Computerized Tomography.* Classics in Applied Mathematics, vol. 32, SIAM, Philadelphia, 2001.

[9] W. Rudin: *Functional Analysis.* International Series in Pure and Applied Mathematics, McGraw-Hill, New-York, 1991.

[10] L.A. Shepp, B.F. Logan: The Fourier reconstruction of a head section. *IEEE Trans. Nucl. Sci.*, **NS-21**, 21–43, 1974.